
Disrupting Deepfakes with an Adversarial Attack that Survives Training

Eran Segalis
Independent Scholar
segaliseran@gmail.com

Abstract

The rapid progress in generative models and autoencoders has given rise to effective video tampering techniques, used for generating deepfakes. Mitigation research is mostly focused on post-factum deepfake detection and not prevention. We complement these efforts by proposing a prevention technique against face-swapping autoencoders. Our technique consists of a novel training-resistant adversarial attack that can be applied to a video to disrupt face-swapping manipulations. Our attack introduces spatial-temporal distortions to the output of the face-swapping autoencoders, and it holds whether or not our adversarial images have been included in the training set of said autoencoders. To implement the attack, we construct a bilevel optimization problem, where we train a generator and a face-swapping model instance against each other. Specifically, we pair each input image with a target distortion, and feed them into a generator that produces an adversarial image. This image will exhibit the distortion when a face-swapping autoencoder is applied to it. We solve the optimization problem by training the generator and the face-swapping model simultaneously using an iterative process of alternating optimization. Finally, we validate our attack using a popular implementation of FaceSwap, and show that our attack transfers across different models and target faces. More broadly, these results demonstrate the existence of training-resistant adversarial attacks, potentially applicable to a wide range of domains.

1 Introduction

Recent improvements in deep learning have contributed to the rise of questionable applications that perform synthetic image rendering, known as deepfakes. They are used maliciously in various ways, from "face swapping" - replacing a person's face in a video with another to misrepresent the target [24] to "face reenactment" [22] - which alters the expressions of a target person in a video by transferring the expressions of a source person to the target.

Efforts to combat such deepfake systems have mostly focused on detection [5, 10, 15, 18, 27, 28, 32], rather than prevention. While identifying content as fraudulent is extremely important, when it comes to content that besmirches a person's reputation - its sole existence might mean the damage is already done, and victims will forever remain affected.

Recently, a new approach to prevent deepfakes has surfaced - implementing adversarial attacks on the malicious deepfake models. An adversarial attack on a given model involves applying minute changes to a given input that are imperceptible by a human, but should the model be applied to the modified input, its output would be erroneous. Two examples of such successful attacks against deepfake systems have been shown in [19, 30].

Such adversarial attacks are effective in defeating deepfakes when the model is unlikely to be trained on data that includes the adversarial samples. Unfortunately, not all scenarios have this constraint.

For example, in a fake news scenario such as [23], a deceiver might train a face-swapping model from scratch on videos of a political figure, in order to swap their face with another. Protecting the political figure’s videos by injecting adversarial samples would cause these samples to be included in the deepfake model’s training set, which could thwart the attack.

In this work, we propose a new family of attacks: **training-resistant adversarial attacks**. These attacks are similarly applied against a given model to produce adversarial samples, but they are a stronger form of adversarial attacks since they survive training. When the attacked model is applied to these samples, it will yield an erroneous output, whether or not these adversarial samples were included in its training data.

We demonstrate such a training-resistant attack against the face-swapping application of deepfake. We chose to focus on this application both because of the increasingly widespread usage of face-swapping in deepfakes, and because face-swapping is a good representative case of a deepfake model, and a successful attack on it could likely be generalized to more applications.

Our attack aims to inject minute perturbations to source video frames, so that when a face-swapping model is applied to them, the output includes visible spatial-temporal distortions that warp it, making the swap evident to a human eye. To achieve this goal and the property of training resistance, we formulate this objective as a general bilevel optimization problem, where we train a face-swapping model instance and an adversarial sample generator against each other; we choose this path over a more specific Minimax problem because we want to avoid modifying the *FaceSwap* autoencoder’s loss function, while keeping the flexibility to modify the adversarial network’s loss function, and direct it toward generating samples that result in effective disruptions.

2 Related Work

Adversarial attacks had been extensively studied in the context of classification problems [1, 2, 4, 8, 12, 14, 16, 20, 25], but less research was published on their effect on generative models and autoencoders [7, 11, 21]. Tabacof *et al.* [7, 21] and Kos *et al.* [11] explore adversarial attacks against Variational Autoencoders (VAE), where Autoencoders and VAE-GAN models are used for image compression. Wang *et al.* [26] adapt adversarial attacks to image-to-image translation tasks under both paired and unpaired settings. Additionally for the paired setting they adapt a poisoning attack on the target domain. Yeh *et al.* [30] and Ruiz *et al.* [19] are two concurrent works to ours, which explore adversarial attacks to disrupt deepfake models. Yeh *et al.* propose a distorting attack in which the image translation model output becomes corrupt and a nullifying attack in which the model becomes the identity mapping. Ruiz *et al.* [19] explore distorting attacks and extend them to conditional image translation networks. Additionally they adapt adversarial training [14] for conditional image translation GANs. Willetts *et al.* [29] explore defenses against adversarial attacks for VAE.

All of these attacks assume that the target models were trained using pristine data, a reasonable assumption for many applications. Unfortunately, for many other deepfake tasks this assumption doesn’t hold. For example, in a face-swapping scenario, a deceiver aims to swap the faces of A and B for some video v_A , which requires training a specific $A \rightarrow B$ model, and therefore collecting the corresponding training data. Since, in this scenario, v_A is available to the deceiver, the training data is likely to include images from v_A - which is the video we aim to protect, and therefore, will contain our adversarial images. Such cases prove a challenge to the attacks proposed by earlier works.

Consequently, an effective attack on this scenario should assume adversarial images might be included in the training data so the attack must be training-resistant, as defined in section 1. On the other hand, unlike in a poisoning attack (where one aims to poison the training data with bad inputs), our training-resistant attack should also assume that they might not be there, and succeed either way. This independence makes our attack much more robust.

In this work, we demonstrate an effective training resistant adversarial attack on face-swapping models. To the best of our knowledge, we are first to introduce a training-resistant adversarial attack in any domain.

3 Method

3.1 DeepFakes generation

While the term deepfake has become synonymous with its result of replacing a face in a video, it also refers to a specific face swapping method. The most notable implementation of this method is [24], as has been analyzed by [18] and many others. In this section, we will briefly describe this implementation of deepfake.

This system receives as input an image sequence featuring source face A (a video, in this context, is viewed as an image sequence), and a sequence featuring target face B. First, an extraction phase extracts the faces from the images, aligns them, and creates masks that indicate where each face is located in each image. Next, two autoencoders with a shared encoder are trained to reconstruct images of the source and target faces. These autoencoders are trained on an augmentation of the input images, created via rotations, translations, magnifications and minute random color changes. Then, they are optimized using a reconstruction loss, which consists of a mask loss and a face loss which is weighted by the input mask. The reconstruction loss is defined as follows:

$$\mathcal{L}_k(x, m) = \|(f_k^{face}(x) - x) \odot m\|_1 + \|f_k^{mask}(x) - m\|_1$$

Where f_k^{face} , f_k^{mask} are the autoencoder face and mask outputs, x is the input image, m is the input mask and \odot denotes a point-wise multiplication. We will refer to this loss as the FaceSwap loss.

This yields an encoder & decoder pair for both face A and face B, where the decoders output both an image and face mask.

Finally, a swapped face is produced by applying the trained encoder and decoder of face B to the target images of face A. The output face is blended into the target image using the face mask.

DeepFake architectures FaceSwap [24] offers several autoencoder architectures and configurations, but training a FaceSwap model is an expensive task that requires several days on high end GPUs. Hence, a full evaluation of all the models is beyond the scope of this paper. Accordingly, we chose 3 architectures for our research:

- **realface**: This architecture uses skip connections for both its encoder and its decoders. It also uses an unbalanced framework where the autoencoder for the target face B has additional layers.
- **dfl-h128**: DeepFaceLab [9] is the one of the most popular deepfake implementations. This model includes a 128×128 pixels input model without skip connections, and closely reassembles the original model implanted in [24].
- **dfl-sae**: Another DeepFaceLab [9] architecture, this one uses skip connections only for the decoders.

These models provide us with diverse architecture types and represent the 2 most popular implementations of deepfake - [24, 9].

3.2 Optimization problem formulation

Our system’s objective is to add a tamper-evident feature to videos, disrupting attempts to manipulate them using deepfake. Thus, for a given video v including the face A , our system will output a modified video v' , where the differences between v and v' are imperceptible to a human observer. However, when the deepfake system is executed on v' with some target face B , the resulting $f_B(v')$ will include, instead of a seamless replacement of A with B , major human-visible artifacts identifying the deepfake tampering performed - thus defeating the attempted face swapping.

To achieve this goal, we use a class of disruptions to modify each frame in video v which are imperceptible in v' , but cause a change in the location, scaling and angle of face B in $f_B(v')$.

To formulate this, we define an adversarial generator $G(x, N)$ which receives as input a face image x and a target affine transformation N . $G(x, N)$ outputs a modified face image satisfying:

$$\begin{aligned} G(x, N) = \arg \min_y \quad & \mathcal{L}_{adv}(y, x, N) \\ \text{s.t.} \quad & \|y - x\|_\infty \leq \varepsilon \end{aligned}$$

Where ε is used to control the magnitude of the adversarial perturbation, which is common in adversarial settings [8], and \mathcal{L}_{adv} is the adversarial loss function defined by:

$$\mathcal{L}_{adv}(y, x, N) = \|f_A^{face}(y) - N(x)\|_1 + \alpha_1 \cdot \|y - x\|_1$$

Where α_1 is used to further minimize the magnitude of the perturbation, and N is an affine transformation operating on x by assigning the pixel $z_{(i,j)}$ the value of:

$$x_{(N_{11} \cdot i + N_{12} \cdot j + N_{13}, N_{21} \cdot i + N_{22} \cdot j + N_{23})}$$

Furthermore, since the autoencoder-predicted face's location and shape is strongly coupled with that of the predicted mask, it is sufficient to define \mathcal{L}_{adv} as:

$$\mathcal{L}_{adv}(y, x, m, N) = \|f_A^{mask}(y) - N(m_x)\|_1 + \alpha_1 \cdot \|y - x\|_1$$

Where m_x is the face's mask.

For the adversarial loss, we use the autoencoder f_A of face A . We do this to keep the adversarial loss an internal process, i.e. defined by face A as much as possible, since an internal process will likely increase the odds for transferability of our adversarial attack to target faces other than B . An alternative we considered was using the predicted mask of f_B for the loss function - however, we cannot assume that f_B^{mask} matches the input mask of face A , and therefore manipulating f_B^{mask} to match $N_x(m_x)$ seems ineffective.

Now, let $\mathcal{D}_A, \mathcal{D}_B$ be the datasets used for training the FaceSwap autoencoders for faces A and B . Let $\mathcal{P}_A \subseteq \mathcal{D}_A$ be the subset of data we can control and would like to protect. For each $(x, m_x) \in \mathcal{P}_A$ we pick a distortion transformation N_x . We aim to find an adversarial generator such that:

$$\begin{aligned} G^* = \arg \min_G \quad & \sum_{(x, m_x) \in \mathcal{P}_A} \mathcal{L}_{adv}(G(x, N_x), x, f_a^{mask}(x), N_x) \\ \text{s.t.} \quad & (f_A, f_B) \in \left\{ \arg \min_{f_A, f_B} \mathcal{L}_B(\mathcal{D}_B) + \mathcal{L}_A(\mathcal{D}_A \setminus \mathcal{P}_A) + \sum_{(x, m_x) \in \mathcal{P}_A} \mathcal{L}_A(G(x, N_x), m_x) \right\} \end{aligned}$$

Remarks An important factor in our problem formulation is the exclusion of the ℓ_∞ constraint. This is due to our design of G , in which we enforce the ℓ_∞ constraint via the network architecture itself.

We chose to use the predicated mask $f_a^{mask}(x)$ for labels in \mathcal{L}_{adv} instead of using the input mask m_x . This choice was made after running our initial experiments, where our expected level of image distortion was not achieved. These results showed that using m_x as label in \mathcal{L}_{adv} causes an unexpected issue with the autoencoder's performance - instead of transforming image x according to N_x , the autoencoder adjusted its predicted mask, making it marginally wider, and with sharper boundaries - thus decreasing the adversarial loss, without achieving the required distortion. This led us to replace m_x with $f_a^{mask}(x)$. This modification forces G to keep trying to increase the image's distortion.

3.3 Training procedure

Next, we proceed to the design of the training algorithm. We begin by constructing, for each x , an affine transformation N_x as $N_x = M_x + I$, where $I = \begin{pmatrix} 1 & 0 & 0 \\ 0 & 1 & 0 \end{pmatrix}$, and M_x is a randomly sampled 2×3 matrix, with its ℓ_∞ norm normalized to be γ , thus ensuring our transformations all have the same magnitude. Specifically, M_x is generated by sampling 6 numbers from a normal distribution with zero mean, and a standard deviation β .

Algorithm 1: Alternating training algorithm

Input: Training data \mathcal{D}_A , \mathcal{D}_B , target training data \mathcal{P}_A , number of epochs N , number of iterations used for training the generator on each batch $BatchIters$, Optimizers Opt_G , Opt_{f_A} , Opt_{f_B} used for training the generator and autoencoders, Affine transformations learning rate θ , Affine transformations ℓ_∞ norm γ

Output: Learned Adversarial Generator G and Affine transformation for each $x \in \mathcal{P}_A$

```
1 for epoch = 1 to N do
2   for i = 1 to number of batches in  $\mathcal{P}_A$  do
3      $b_x, b_m, b_N \leftarrow \mathcal{P}_A$ -batch: images, mask and transformations
4      $b_m^{predicted} \leftarrow f_A^{mask}(b_x)$ 
5     for k = 1 to BatchIters do
6        $b_N \leftarrow SGD(b_N, b_x, b_m^{predicted}, \theta)$  // Optimize  $N$ 
7        $b_N \leftarrow Project(b_N, \gamma, I)$  // Project  $N_x$  to the  $\gamma$  sphere around  $I$ 
8     end
9     for  $m_x$  in  $b_m^{predicted}$  do
10       $b'_{m,x} \leftarrow N_x(m_x)$  // Prepare the distorted mask labels for the adversarial loss
11    end
12    for k = 1 to BatchIters do
13       $G \leftarrow opt_G(b_x, b_N, b'_{m,x})$  // Train  $G$  on batch
14    end
15     $b_x^{adv} \leftarrow G(b_x, b_N)$ 
16     $b_x^{aug}, b_m^{aug} \leftarrow Augment(b_x^{adv}, b_m)$ 
17     $f_A \leftarrow opt_{f_A}(b_x^{aug}, b_m^{aug})$ 
18
19     $c_x^{aug}, c_m^{aug} \leftarrow \text{Augmented } \mathcal{D}_B\text{-batch images and masks}$ 
20     $f_B \leftarrow opt_{f_B}(c_x^{aug}, c_m^{aug})$ 
21  end
22  for i = 1 to number of batches in  $(\mathcal{D}_A \setminus \mathcal{P}_A)$  do
23     $b_x^{aug}, b_m^{aug} \leftarrow \text{Augmented } \mathcal{D}_A\text{-batch images and masks}$ 
24     $f_A \leftarrow opt_{f_A}(b_x^{aug}, b_m^{aug})$ 
25
26     $c_x^{aug}, c_m^{aug} \leftarrow \text{Augmented } \mathcal{D}_B\text{-batch images and masks}$ 
27     $f_B \leftarrow opt_{f_B}(c_x^{aug}, c_m^{aug})$ 
28  end
29 end
30 return  $G$  and  $N_x$  for each  $x \in \mathcal{P}_A$ 
```

In order to optimize N_x , we introduce another loss function. This function should target an increase in our spatial-temporal video distortions - as such it should aim to maximize the variance of N_x across our target dataset \mathcal{P}_A . In addition, for each image x we'd like to find the affine transformation most likely to succeed in manipulating the face's location, angle and shape, while assuming that N_x belongs to the ℓ_∞ sphere of radius γ around I . Consequently, we define our new loss function to be:

$$\mathcal{L}_{noise}(b_N, \mathcal{B}) = -\alpha_2 \cdot \sigma(b_N) - \frac{1}{|\mathcal{B}|} \sum_{(x, m_x) \in \mathcal{B}} \|f_A^{mask}(G(x, N_x)) - N_x(f_A^{mask}(x))\|_1$$

Where \mathcal{B} is a batch of face images and masks, b_N is a batch of affine transformations N_x , and σ is the standard deviation of b_N .

For the next part of the training algorithm, we note that our bilevel optimization problem is closely related to the one used in poisoning attacks such as [17]. Therefore, we similarly solve the optimization problem by running an iterative process of alternating optimization of both G (via the adversarial loss \mathcal{L}_{adv}) and f_A, f_B (via the FaceSwap losses $\mathcal{L}_A, \mathcal{L}_B$).

Finally, in order to stabilize the training process and to achieve stronger distortions of the output, we allow our generator extra training cycles for each batch we train on. The resulting algorithm is summarized in Algorithm 1.

Network architecture For our adversarial generator, we choose to rely on the work in [2, 6] and use an autoencoder architecture. Specifically, we adapted the dfl-h128 autoencoder used in FaceSwap [24], which we’ve chosen since it is the model we train against in Algorithm 1. To address the ℓ_∞ constraint, we use \tanh non-linearity in our last convolutional layer and multiply the result by ε . A detailed description of the generator network’s architecture is shown in figure 1.

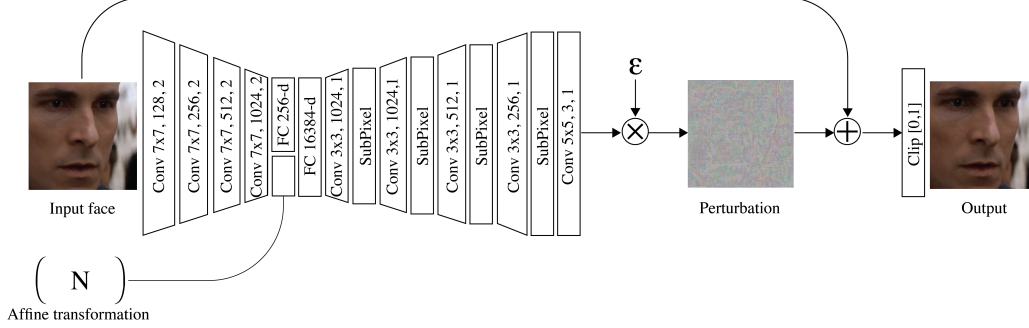


Figure 1: The architecture of our generator.

4 Experiments

We evaluate our attack against the face-swapping models described in section 3.1, with some slight adjustments so the models would have the same input size and they could be trained with the same batch size while fitting in our GPU’s memory. First, we match the input size of the realface model to 128×128 . Next, we slightly decrease the sizes of realface (by setting `dense_nodes` to 1408) and dfl-h128 (by setting `low_memory=True`). This decrease in size should not affect the efficacy of our technique on the original models.

Datasets We collected several videos from YouTube for 3 people A, B, C . For each person, we first extracted their face images from the videos using S³FD [31] and aligned them using FAN [3]. Then, we removed blurry images and the face images of other people appearing in the videos. This resulted in a set of about 5000 face images for each person. For our dataset \mathcal{P}_A , we arbitrarily choose person A and focus on the subset of 444 face A images extracted from one of their videos, v_A .

4.1 Generation of adversarial images

We train the adversarial generator against a low-memory version of the dfl-h128 model using Algorithm 1, with the following hyperparameters: $\varepsilon = \frac{2}{255}$, $\alpha_1 = \frac{3}{255}$, $\alpha_2 = 0.012$, $\beta = 0.15$, $\gamma = 0.225$, `BatchIters` = 8. To optimize the affine transformations, we use a learning rate of $\theta = 0.001$. All of the networks were trained using the Adam optimizer with the following hyperparameters: $\beta_1 = 0.9$, $\beta_2 = 0.9999$, a learning rate of 5×10^{-5} and a batch size of 64. The generator has been trained for 1024 epochs using \mathcal{D}_A , \mathcal{P}_A and \mathcal{D}_B . As explained in Algorithm 1 above, this results in the trained adversarial generator, as well as output affine transformations.

Next, we use these generator and transformations to calculate the adversarial images of the face images in \mathcal{P}_A , and we patch them back onto their original video v_A resulting in the adversarial video v'_A . As before, we extract and align face images using S³FD and FAN from v'_A and merge these images with rest of face A s images (without the pristine face images from v_A). We call this new dataset \mathcal{D}'_A .

4.2 Evaluation

We first evaluate our attack against face swapping models trained using the dataset \mathcal{D}'_A , which includes our adversarial images. We trained the dfl-h128 model for the task of face swapping $A \rightarrow B$. Additionally, in order to evaluate the transferability of our attack across architectures, we trained both the dfl-sae and realface models for $A \rightarrow B$. We trained another dfl-h128 model for $A \rightarrow C$

to also evaluate the transferability across different target faces. All models were trained for 200000 iterations using the Adam optimizer with the following hyperparameters: $\beta_1 = 0.5$, $\beta_2 = 0.999$, a learning rate of 5×10^{-5} and a batch size of 64. The training was executed using the FaceSwap code [24] using its default hyperparameters, and the same number of training iterations as were used to generate the FaceForensics dataset [18], which is used for the detection of face swapped videos.

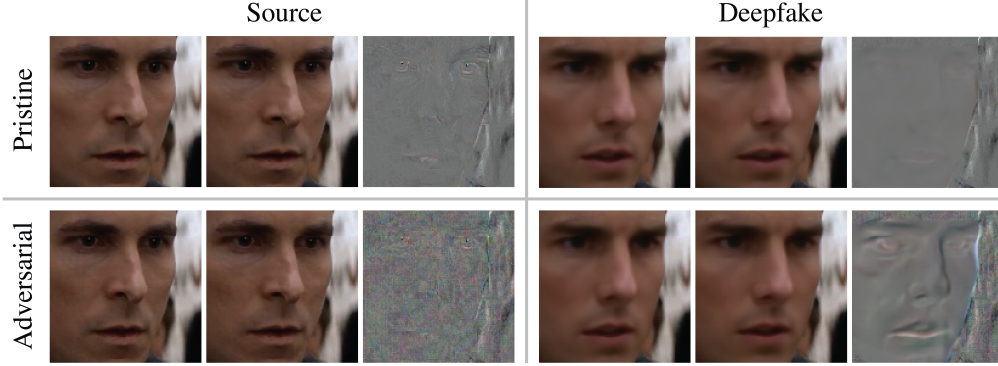


Figure 2: Samples from dfl-h128 model trained for 500000 iterations on $\mathcal{D}'_{\mathcal{A}}$. First row from left to right: Pristine consecutive face images from our video, visualization of their difference, their face swapping output and a visualization of its difference. Second row from left to right: adversarial perturbations of the same consecutive images, visualization of their difference, their face swapping output and a visualization of its difference.

Figure 2 shows that injecting the adversarial perturbations to the pristine video creates a difference between consecutive frames that’s similar to white noise added to the natural difference between the matching pristine frames - this is why the perturbations are not observable in the adversarial source video. However, the difference between consecutive frames of this video after a deepfake model is applied to it resembles a face - this is because the attack caused the face’s location to shift. This shift is noticeable in the disrupted video, as can be seen in the video in the supplementary material¹.

Spatial-temporal score A more quantitative way to measure the video distortion, is to calculate the average ℓ_2 distance between consecutive video frames of the face swapped video. However, since regular consecutive video frames exhibit a natural spatial-temporal difference, we normalize the score to account for this differences. Consequently, our spatial-temporal score will be defined as the ratio of the distortion scores of the modified and original videos. Formally, let f_k be our face swapping autoencoder, let x_i be the face images from v_A , and x'_i be the face images from v'_A . We define y_i, y'_i to be the face swapped images of x_i, x'_i by f_k (calculated using the predicted face and mask of f_k as described in section 3), and finally we define the spatial-temporal score of f_k as:

$$s(f_k) = \frac{\sum_{i=1}^{n-1} \|y'_{i+1} - y'_i\|_2}{\sum_{i=1}^{n-1} \|y_{i+1} - y_i\|_2}$$

Having defined the spatial-temporal score metric, we can analyze the score of our attack, as applied to the various models - see Table 1. These results show that even though the face swapping models’ training data included our adversarial images, our attack successfully created major artifacts in the resulting video, increasing the average ℓ_2 distance between consecutive images by at least 4.1%.

Next, we validate that our attack is successful even when our adversarial images are excluded from the training set $\mathcal{D}_{\mathcal{A}}$, thus confirming that our attack is training-resistant, rather than a poisoning attack which requires injecting samples into the training process. We train dfl-h128, dfl-sae and realface on $\mathcal{D}_{\mathcal{A}} \setminus \mathcal{P}_{\mathcal{A}}$ and $\mathcal{D}_{\mathcal{B}}$ for $(A \rightarrow B)$, and another dfl-h128 model for $A \rightarrow C$. Training is performed in the same way described before, and the spatial-temporal score is calculated for each model. As expected - the spatial-temporal scores appearing in Table 2 are much higher than in Table 1, which is also reflected in the greater magnitude of the distortions seen in the second demo video².

¹See the first demo video in <https://youtu.be/x01XKQp4pks>

²See the second demo video in <https://youtu.be/kk7DS3VCvPk>

Table 1: Spatial-temporal scores for models trained for 200000 iterations on a dataset which includes our adversarial images.

Architecture	Swapping direction	Spatial-temporal score
dfl-h128	$A \rightarrow B$	1.048
dfl-h128	$A \rightarrow C$	1.041
dfl-sae	$A \rightarrow B$	1.058
realface	$A \rightarrow B$	1.048

Table 2: Spatial-temporal scores for models trained for 200000 iterations on a pristine dataset.

Architecture	Swapping direction	Spatial-temporal score
dfl-h128	$A \rightarrow B$	1.135
dfl-h128	$A \rightarrow C$	1.133
dfl-sae	$A \rightarrow B$	1.155
realface	$A \rightarrow B$	1.092

Finally, we investigate the effect of extra training on \mathcal{D}'_A . We train our dfl-h128 model on the task $A \rightarrow B$ for another 300000 iterations, and calculate the spatial-temporal score every 25000 iterations. As shown in Figure 3, the spatial-temporal score begins to stabilize after 300000 iterations, and even after 500000 iterations it remains larger than 1.0 with a value of 1.029. These distortions are still highly noticeable, as can be observed in Figure 2. This confirms that even a resourceful deceiver will fail in manipulating v'_A due to our attack.

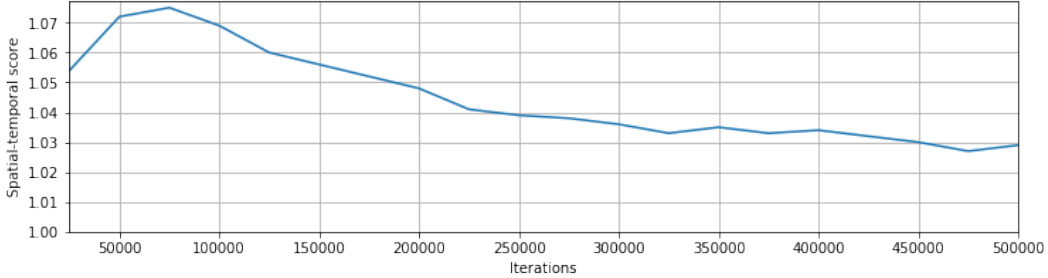


Figure 3: Spatial-temporal scores for dfl-h128 model trained on the task $A \rightarrow B$ for 500000 iterations.

5 Conclusions

In this work we introduced the notion of a training-resistant adversarial attack. Such an attack generates adversarial samples against a given model such that when the model is applied to these samples, the model’s intended effect is disrupted - even if the same adversarial samples were part of the model’s training data. This is a key difference between this family of attacks and poisoning attacks, since poisoning attacks require that the adversarial samples be part of the training data.

Additionally, we applied such a training-resistant adversarial attack against face-swapping autoencoders. We then successfully validated our results against a commonly used FaceSwap implementation [24], and showed that our attack transfers across different models and target faces. Therefore, we believe that our technique can be applied to other deepfake autoencoders, which opens interesting new avenues for disrupting deepfake models for future research.

These results demonstrate the existence and feasibility of training-resistant adversarial attacks, potentially applicable to a wide range of domains.

Acknowledgements

The authors would like to thank Jonathan Heimann and Roy Iarchy for many fruitful discussions and comments.

Broader Impact

Image manipulation based deepfakes is already being used for malicious applications, from the synthesis of non-consensual pornography [13], to fraudulent attempts to misrepresent politicians and influencing the democratic process itself, as happened in Belgium in 2020 [23]. A technique to protect videos against image manipulation would be a boon in these circumstances, providing much-needed protection. However, a malicious attacker could apply our technique to other, benevolent cases of image-to-image transfer learning, with negative consequences. For example, Wang *et al.* in [26] discuss disrupting the performance of self-driving cars using an adversarial attack on the datasets used to train the vehicles; our training-resistant technique could make such attacks more feasible to malicious attackers, interfering with the performance of self driving cars.

More broadly, the advent of training-resistant adversarial attacks presents a challenge to Deep Neural Networks (DNNs) in general. Today, a common method for improving the robustness of critical DNN models involves training them on adversarial examples, as in [14]. Future work might generalize training-resistant adversarial attacks to succeed in subverting such a model, even if it has trained on their adversarial examples. For example, a piece of malicious software could evade an anti-virus model trained to classify code as malicious or benign, despite the model being trained on intercepted samples of the malicious software itself.

On the other hand, as we show in our implementation, training-resistant adversarial attacks can be used to foil a malicious application of a DNN by protecting its possible targets; in fact, our research shows how a method with traditionally malicious applications towards DNNs (adversarial attacks) can be implemented in a way that protects data against manipulation by an unethical applications of a DNN. As such, we believe that while these novel attacks do carry some risk, their potential for defeating malicious applications of DNNs make them an exciting and relevant field of study in the modern machine learning landscape.

References

- [1] Naveed Akhtar and Ajmal Mian. Threat of adversarial attacks on deep learning in computer vision: A survey, 2018.
- [2] Shumeet Baluja and Ian Fischer. Adversarial transformation networks: Learning to generate adversarial examples, 2017.
- [3] Adrian Bulat and Georgios Tzimiropoulos. How far are we from solving the 2d & 3d face alignment problem? (and a dataset of 230,000 3d facial landmarks). In *International Conference on Computer Vision*, 2017.
- [4] Nicholas Carlini and David Wagner. Towards evaluating the robustness of neural networks, 2016.
- [5] Davide Cozzolino, Justus Thies, Andreas Rössler, Christian Riess, Matthias Nießner, and Luisa Verdoliva. Forensictransfer: Weakly-supervised domain adaptation for forgery detection, 2018.
- [6] Ji Feng, Qi-Zhi Cai, and Zhi-Hua Zhou. Learning to confuse: Generating training time adversarial data with auto-encoder, 2019.
- [7] George Gondim-Ribeiro, Pedro Tabacof, and Eduardo Valle. Adversarial attacks on variational autoencoders, 2018.
- [8] Ian J. Goodfellow, Jonathon Shlens, and Christian Szegedy. Explaining and harnessing adversarial examples, 2014.
- [9] iperov. Deepfacelab github., 2020. URL <https://github.com/iperov/DeepFaceLab>.

- [10] Ali Khodabakhsh, Raghavendra Ramachandra, Kiran Raja, Pankaj Wasnik, and Christoph Busch. Fake face detection methods: Can they be generalized? In *2018 International Conference of the Biometrics Special Interest Group (BIOSIG)*, pages 1–6. IEEE, 2018.
- [11] Jernej Kos, Ian Fischer, and Dawn Song. Adversarial examples for generative models, 2017.
- [12] Alexey Kurakin, Ian Goodfellow, and Samy Bengio. Adversarial examples in the physical world, 2016.
- [13] Dave Lee. Deepfakes porn has serious consequences, 2020. URL <https://www.bbc.com/news/technology-42912529>.
- [14] Aleksander Madry, Aleksandar Makelov, Ludwig Schmidt, Dimitris Tsipras, and Adrian Vladu. Towards deep learning models resistant to adversarial attacks, 2017.
- [15] Francesco Marra, Diego Gragnaniello, Davide Cozzolino, and Luisa Verdoliva. Detection of gan-generated fake images over social networks. In *2018 IEEE Conference on Multimedia Information Processing and Retrieval (MIPR)*, pages 384–389. IEEE, 2018.
- [16] Seyed-Mohsen Moosavi-Dezfooli, Alhussein Fawzi, Omar Fawzi, and Pascal Frossard. Universal adversarial perturbations, 2016.
- [17] Luis Muñoz-González, Battista Biggio, Ambra Demontis, Andrea Paudice, Vasin Wongrasamee, Emil C. Lupu, and Fabio Roli. Towards poisoning of deep learning algorithms with back-gradient optimization, 2017.
- [18] Andreas Rössler, Davide Cozzolino, Luisa Verdoliva, Christian Riess, Justus Thies, and Matthias Nießner. Faceforensics++: Learning to detect manipulated facial images. *CoRR*, abs/1901.08971, 2019.
- [19] Nataniel Ruiz, Sarah Adel Bargal, and Stan Sclaroff. Disrupting deepfakes: Adversarial attacks against conditional image translation networks and facial manipulation systems, 2020.
- [20] Christian Szegedy, Wojciech Zaremba, Ilya Sutskever, Joan Bruna, Dumitru Erhan, Ian Goodfellow, and Rob Fergus. Intriguing properties of neural networks, 2013.
- [21] Pedro Tabacof, Julia Tavares, and Eduardo Valle. Adversarial images for variational autoencoders, 2016.
- [22] Justus Thies, Michael Zollhofer, Marc Stamminger, Christian Theobalt, and Matthias Nießner. Face2face: Real-time face capture and reenactment of rgb videos. In *Proceedings of the IEEE conference on computer vision and pattern recognition*, pages 2387–2395, 2016.
- [23] Rob Toews. Deepfakes are going to wreak havoc on society. we are not prepared., 2020. URL <https://www.forbes.com/sites/robtoews/2020/05/25/deepfakes-are-going-to-wreak-havoc-on-society-we-are-not-prepared/#2248f32b7494>.
- [24] Torzdf. Deepfakes github., 2020. URL <https://github.com/deepfakes/faceswap>.
- [25] Florian Tramèr, Alexey Kurakin, Nicolas Papernot, Ian Goodfellow, Dan Boneh, and Patrick McDaniel. Ensemble adversarial training: Attacks and defenses, 2017.
- [26] Lin Wang, Wonjune Cho, and Kuk-Jin Yoon. Deceiving image-to-image translation networks for autonomous driving with adversarial perturbations. *IEEE Robotics and Automation Letters*, 5(2):1421–1428, Apr 2020. ISSN 2377-3774. doi: 10.1109/lra.2020.2967289. URL <http://dx.doi.org/10.1109/LRA.2020.2967289>.
- [27] Run Wang, Felix Juefei-Xu, Lei Ma, Xiaofei Xie, Yihao Huang, Jian Wang, and Yang Liu. Fakespotter: A simple yet robust baseline for spotting ai-synthesized fake faces, 2019.
- [28] Sheng-Yu Wang, Oliver Wang, Richard Zhang, Andrew Owens, and Alexei A. Efros. Cnn-generated images are surprisingly easy to spot... for now, 2019.

- [29] Matthew Willetts, Alexander Camuto, Tom Rainforth, Stephen Roberts, and Chris Holmes. Improving vaes' robustness to adversarial attack, 2019.
- [30] Chin-Yuan Yeh, Hsi-Wen Chen, Shang-Lun Tsai, and Sheng-De Wang. Disrupting image-translation-based deepfake algorithms with adversarial attacks. In *Proceedings of the IEEE Winter Conference on Applications of Computer Vision Workshops*, pages 53–62, 2020.
- [31] Shifeng Zhang, Xiangyu Zhu, Zhen Lei, Hailin Shi, Xiaobo Wang, and Stan Z. Li. S³fd: Single shot scale-invariant face detector, 2017.
- [32] Peng Zhou, Xintong Han, Vlad I. Morariu, and Larry S. Davis. Two-stream neural networks for tampered face detection, 2018.